COO-3077-231

# ELASTIC NEUTRINO PROTON AND ANTINEUTRINO PROTON SCATTERING*

Alan B. Entenberg
Physics Department, 2El - D.R.L.
University of Pennsylvania
Philadelphia, Pennsylvania 19104

and

D. Cline, E. Egelman, J. Horstkotte, W. Kozanecki,
A. K. Mann, D. D. Reeder, C. Rubbia, J. Strait,
L. Sulak, P. Wanderer, H. H. Williams, M. Yudis
(Harvard University, University of Pennsylvania,
University of Wisconsin, Brookhaven National Laboratory)



Abstract: Distributions of $dN/dQ^2$ for $\sim 150$ events of the process $\nu_\mu p \to \nu_\mu p$ and for $\sim 40$ events of $\bar{\nu}_\mu p \to \bar{\nu}_\mu p$ are shown in the region $0.35 \leq Q^2 \leq 0.9$ $(GeV/c)^2$ where $-Q^2$ is the square of the four momentum transferred from the incident neutrino to the proton. Preliminary estimates of the weak neutral current to weak charged current ratios from these data are consistent with the values of $R_\nu = 0.17 \pm 0.05$ and $R_{\bar{\nu}} = 0.2 \pm 0.1$ measured by us previously.

Resume: Les distributions de $dN/dQ^2$ pendant $\sim 150$ incidents du procédé $\nu_\mu p \to \nu_\mu p$ et pendant $\sim 40$ incidents de $\bar{\nu}_\mu p \to \bar{\nu}_\mu p$ se trouvent dans la région $0.35 \leq Q^2 \leq 0.9$ $(GeV/c)^2$ ou $-Q^2$ est le carré du four-momentum transféré du neutrino incidentiel au proton. Les évaluations préliminaires de la proportions du courant neutri au courant chargé s'accordent aussi a leurs valeurs antérieures du $R_\nu = 0.17 \pm 0.05$ et $R_{\bar{\nu}} = 0.2 \pm 0.1$.

* Work supported in part by the U. S. Energy Research and Development Administration.

Paper presented at International Meeting on High Energy Leptonic Interactions, XII Rencontre De Moriond, Flaine-Haute Savoie-France, March 6-11, 1977.

## DISCLAIMER

Introduction

The simplest manifestation of the weak hadronic current occurs in the neutral current "NC" elastic scattering channel: $\nu_\mu + p \rightarrow \nu_\mu + p$. Two independent variables describe this process: $E_\nu$, the incident neutrino energy, and $Q^2$, the negative square of the four momentum transferred from the lepton to the nucleon. In practice, only T and $\psi$, the kinetic energy and recoil angle of the proton, are measurable (see below).

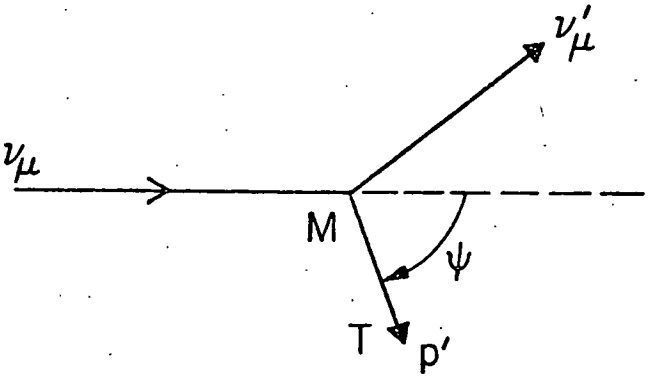


From T and $\psi$, $E_\nu$ and $Q^2$ may be constructed.

$$Q^2 = -q_\mu \cdot q_\mu = 2MT$$

$$E_\nu = \frac{M}{(\cos\psi \cdot \sqrt{1 + \frac{2M}{T}} - 1)}$$

At present, the dynamics of neutral current elastic scattering are not fully understood. The framework in which one usually works is the "current-current" formalism which is common to theories of weak and electromagnetic interactions. The weak interaction hamiltonian involves a product of the neutral leptonic and neutral hadronic currents:

$$H_w = \frac{G_\beta}{\sqrt{2}} \; j_\lambda \cdot J_\lambda \quad , \; G_\beta = \frac{10^{-5}}{M^2}$$

The precise space-time structures of $j_\lambda$, the leptonic current, and $J_\lambda$, the hadronic current, may be determined from $\nu_\mu p$ and $\bar{\nu}_\mu p$ elastic scattering data interpreted in the context of a particular theory.

In the Weinberg-Salam model[3], the currents $j_\lambda$ and $J_\lambda$ have a natural form. Both neutral currents possess a space-time structure which is a mixture of Vector and Axial-vector. (Recall that the parity violating "V-A" combination successfully describes the charged-current "CC" quasi-elastic reactions, $\nu_\mu n \to \mu^- p$ and $\bar{\nu}_\mu p \to \mu^+ n$.[4]) Neutral and charged currents are related through "weak isospin" rotations; this requirement leads to a maximum relative rate of 0.25 for $R_\nu \equiv \frac{\sigma(\nu p \to \nu p)}{\sigma(\nu n \to \mu^- p)}$ and $R_{\bar{\nu}}$ for anti-neutrinos. Finally, the model allows for the unification of the weak and electromagnetic interactions via the Weinberg angle, $\theta_w$, which mixes the weak and electromagnetic currents.

The matrix element of the neutral hadronic current may be written as follows

$$< p|J_\lambda|p > = \bar{u}_p [ (g_v^o + g_A^o \cdot \gamma_5) \gamma_\lambda + i (p_\lambda + p'_\lambda) \cdot f_v^o ] u_p - 2 \sin^2\theta_w <p|J_\lambda^{e-m}|p>$$

The Weinberg angle is the only free parameter in the theory since $g_v^o, f_v^o$ are related to the "dipole" form-factors measured in elastic ep and en scattering; $g_A^o$, determined from quasi-elastic neutrino data, has a dipole structure characterized by a mass $M_A \approx 0.9$ GeV.

The experiment described herein tests the basic assumptions which underlie the Weinberg-Salam model: (1) mixed V,A structure of the weak neutral current, (2) the existence of a weak isospin symmetry, and (3) the mixing of weak and electromagnetic currents via the angle $\theta_w$.

Experimental Setup

The method for isolating the elastic channels is intended to overcome the problems of low statistics and high neutron background. The intense, low energy, Brookhaven neutrino beam (Fig. 1) and the massive Harvard-Pennsylvania-Wisconsin target detector (Fig. 2a) together provide adequate rate. The beam has an intensity of $\sim 10^{10} \nu_\mu$/ (3m x 3m) distributed in 12 RF correlated bunches of width 40 nsec; the antineutrino flux is approximately one-half the neutrino flux.[5]

The target detector consists of 30 tons of liquid scintillator contained in 12 calorimeter modules; 4 drift chamber supermodules (2 "X" and

2"Y" planes) are interspersed at the downstream end; a veto counter at the front provides rejection against entering charged particles. The setup can be used to measure both the ionization energy loss and angle of a charged particle moving through the detector. Each calorimeter (Fig. 2b) is optically divided into two "slabs" each of 8 fiducial cells (19 cm x 23 cm x 266 cm) and upper and lower cells (38 cm x 46 cm x 266 cm) which can be used via software to insure vertical containment of ionization energy loss. Altogether, there are 192 fiducial cells and a fiducial mass of 10 tons. Each cell is equipped with photomultiplier tubes at both ends, the pulses from which are discriminated, timed, and pulse-height analyzed. The hodoscopic nature of each calorimeter provides vertical and longitudinal resolution of ionization position to within $\pm$ 10 cm and the difference in photo-pulse arrival times at either end of a given cell provides horizontal resolution to within $\pm$ 15 cm. Single track identification is facilitated at the downstream end via the four drift chamber supermodules each capable of determining position ($\pm$ 1 mm) and angle ($\pm$ 1°) for a single track.

The cellular nature of the apparatus also allows particle identification using known $\frac{dE}{dX}$ information to interpret energy distribution patterns of ionizing tracks. Pulse-height calibration is done with vertical minimum ionizing cosmic ray muons which leave an average energy of 42 MeV in each cell.

Neutron Rejection

To minimize neutron background the apparatus is entirely enclosed in a heavy-concrete blockhouse with walls 1.2 meters thick. Further, precise event timing ($\pm$ 1 nsec) is used to check the correlation of each event with the RF structure of the fast extracted beam (Figure 6a). Neutrino induced events will occur close ($\pm$ 30 nsecs) to the center of an RF peak; events coming from slower moving neutrons will be evenly distributed during the beam spill. Finally, the technique of using the outer regions of the liquid to "actively shield" the fiducial volume imposes a characteristic "second cluster of energy" signature on neutron-induced events. The size of the detector makes it unlikely that a

neutron can enter the fiducial region, scatter, and exit without scattering a second time. Hence, rejection of neutron induced events is enhanced by eliminating events with second energy depositions in excess of 10 MeV.

Particle Identification

Good particle identification requires a particle to have had a minimum range or energy with which to provide sufficient $\frac{dE}{dX}$ information. In Figure 3 the observed energy deposition pattern for a 225 MeV particle is shown; calculated patterns for a proton and a pion are also shown. The agreement between the data and the pion hypothesis identifies the track as that of a pion. In Figure 4, a proton hypothesis is favored for a 299 MeV particle moving at an angle of 25° through the liquid. Not all patterns are as easily recognized; hence a $\chi^2$-like parameter is used to measure the degree to which a given energy deposition pattern fits a proton or a pion hypothesis. Generally, for an energy deposition in excess of 150 MeV, a reliable separation of protons from pions can be achieved.

Data

A deposition of 5 MeV or more of ionization energy in the liquid during the 3 μsec beam spill triggered the readout of all calorimeter and drift-chamber information. Approximately 1 in 2000 $\nu_\mu$ triggers ( 1 in 8,000 $\bar{\nu}_\mu$ triggers) survives the selection criteria described in Table 1 which are designed to isolate the NC elastic channel. Samples of data which pass and are expected to pass these cuts are listed in the following table.

Event Statistics

| Sample | $\nu_\mu p \to \nu_\mu p$ | $\bar{\nu}_\mu p \to \bar{\nu}_\mu p$ |
|---|---|---|
| Published 1976[1,2] | 30 (7 background) | 22 (8 background) |
| Analyzed to date Reporting now | ~ 150 | ~ 40 |
| Remaining to be analyzed | ~ 150 | ~ 40 |
| Approved running now in progress | ~ 150 | ~ 100 |
| Total ( Dec. 1977) | ~ 450 | ~ 200 |

The data to be presented here are the "analyzed to date" samples of ~ 150 $\nu_\mu$ events and ~ 40 $\bar{\nu}_\mu$ events. The sample of $\nu_\mu$ events is represented kinematically in the scatter-plot of proton kinetic energy versus proton angle shown in Figure 5. That this sample (and that from $\bar{\nu}_\mu$ whose distributions possess the same features) is largely $\nu_\mu$-induced as opposed to n-induced is indicated by the following arguments. The events are in time with the neutrino beam whose RF structure is shown in Figure 6A. The fine timing distribution in which the time of each event from the center of its associated RF bunch is plotted in the cross-hatched region of Figure 6b; a sample of known $\nu_\mu$-induced quasi-elastic events is also shown to illustrate the correlation of the elastic sample with the beam. Finally, the transverse and longitudinal distributions of event vertices show no evidence of characteristic neutron attenuation from either the sides or the front of the detector (see Figures 7a and 7b).

The majority of protons have recoil angles in excess of 20°, a characteristic which from the standpoint of dynamics is inconsistent with the forward-backward peaked scattering of neutrons on protons; moreover, the incident neutrino energy band, within which these events lie, overlaps the region of the Brookhaven neutrino spectrum shown in Figure 1 which peaks at ~ 1 GeV and falls off by one-half at 0.3 GeV and 2.0 GeV.

Backgrounds

Estimated n-induced and $\nu_\mu$-induced backgrounds are listed in Table 2. The former represents the contribution of the flat background (Figure 6b) of out-of-time, potentially n-induced, events which underlie the in-time sample. The latter represent 2 prong ($\mu^- p$) and 2 cluster ($\nu_\mu \pi^\circ p$, $\nu_\mu \pi^+ n$) events in which only a single track was detected and in which dE/dX information was consistent with that of a heavily ionizing proton. Detailed discussions of these backgrounds are in references 1 and 2.

Results

Our previously published[1,2] NC elastic distributions of $dN/dQ^2$ which have been normalized to CC quasi-elastic data for $\nu_\mu$ and $\bar{\nu}_\mu$ are shown in Figures 8a and 9a respectively. To the right, in Figures 8b and 9b, are the unnormalized, detection-efficiency corrected, $Q^2$ distributions for $\sim 150$ $\nu_\mu p \rightarrow \nu_\mu p$ and $\sim 40$ $\bar{\nu}_\mu p \rightarrow \bar{\nu}_\mu p$ in which the statistical fluctuations of the earlier data are absent. Backgrounds have not been subtrated from these samples, but they are expected to have small effect in the region $0.35 \leq Q^2 \leq 0.9$ $(GeV/c)^2$. Preliminary estimates of the ratio of NC elastic to CC quasi-elastic cross-sections do not differ significantly from their earlier values of

$$R_\nu = \frac{\sigma(\nu p \rightarrow \nu p)}{\sigma(\nu n \rightarrow \mu^- p)} = 0.17 \pm 0.05 \qquad 0.3 \leq Q^2 \leq 0.9 \ (GeV/c)^2 \qquad \text{(Ref. 1)}$$

$$R_{\bar{\nu}} = \frac{\sigma(\bar{\nu} p \rightarrow \bar{\nu} p)}{\sigma(\nu p \rightarrow \mu^+ n)} = 0.2 \pm 0.1 \qquad 0.3 \leq Q^2 \leq 0.9 \ (GeV/c)^2 \qquad \text{(Ref. 2)}$$

and confirm our earlier result that $\sigma(\nu_\mu p \rightarrow \nu_\mu p) \neq \sigma(\bar{\nu}_\mu p \rightarrow \bar{\nu}_\mu p)$.

Conclusions[6]

In the context of the Weinberg model, the result that $\sigma(\nu_\mu p \rightarrow \nu_\mu p) \neq \sigma(\bar{\nu}_\mu p \rightarrow \bar{\nu}_\mu p)$ implies that the Dirac space-time structure of the weak hadronic neutral current cannot be pure polar vector (V) or pure axial-vector (A) in form, since

$$\left(\frac{d\sigma^\nu}{dQ^2} - \frac{d\sigma^{\bar{\nu}}}{dQ^2}\right)_E = \frac{G^2}{\pi M} \cdot \frac{Q^2}{E} \cdot \left(1 - \frac{Q^2}{4\pi E}\right) \cdot g_A^o \cdot g_V^o$$

$$> 0 \quad \text{implies } g_A^o \neq 0 \text{ and } g_V^o \neq 0$$

Our published data are consistent with a mixture of V and A, as hypothesized by Weinberg and Salam, and yield a value of $\sin^2 \theta_w \approx 0.2 \pm 0.1$ as shown in Figure 10. Pure vector models appear unlikely as is also indicated in Fig. 10.

Table 1

Selection Criteria for Preliminary Sample

| Criterion | Motivation |
|---|---|
| 1. Fiducial Containment of ionization<br>-80 cm ≤ Horizontal position ≤ 80 cm<br>1 ≤ Vertical cell ≤ 8<br>5 ≤ Longitudinal slab ≤ 23 | Interaction neutral induced<br>Valid measurement of $Q^2$ = 2 MT |
| 2. Event in time with $\nu_\mu$ beam<br>$-30\text{nsec} \leq t_{EVENT} - t_{RF\ peak} \leq 30\text{nsec}$ | Interaction neutrino-induced as opposed to slow neutron induced |
| 3. Non-contiguous excess energy < 10 MeV | Use active shielding technique to minimize n-induced events and $\nu_\mu$-induced $\nu_\mu \pi^+ n$, $\nu_\mu \pi^\circ p$ background final states. |
| 4. Event must lie within at least 3 fiducial cells | Insure adequate angular resolution |
| 5. Ionization energy ≥ 187 MeV | Optimize separation of protons and pions; further minimize n-induced events |

Table 2

Preliminary Background Estimates

| | $\nu_\mu p \to \nu_\mu p$ | $\bar{\nu}_\mu p \to \bar{\nu}_\mu p$ |
|---|---|---|
| $np \to np$ | $\lesssim 10\%$ | $\lesssim 20\%$ |
| $\nu p \to \nu p\pi^o$<br>$\bar{\nu} p \to \bar{\nu} p\pi^o$ | $\lesssim 5\%$ | $\lesssim 5\%$ |
| $\nu n \to \nu p\pi^-$<br>$\bar{\nu} n \to \bar{\nu} p\pi^-$ | $\lesssim 3\%$ | $\lesssim 3\%$ |
| $\nu n \to \mu^- p$<br>$\bar{\nu} p \to \mu^+ n$ | $\lesssim 3\%$ | $\lesssim 3\%$ |
| Cosmic Rays | $\sim 0\%$ | $\sim 0\%$ |
| $\nu n \to \nu n (np \to np)$<br>$\nu p \to \nu p (pn \to pn)$<br>nuclear effects | $\lesssim 10\%$ | $\lesssim 10\%$ |

## REFERENCES


1. D. Cline, A. Entenberg, W. Kozanecki, A.K. Mann, D.D. Reeder, C. Rubbia, J. Strait, L. Sulak, and H.H. Williams, Phys. Rev. Lett. 37, 252 (1976).
2. D. Cline et al, Phys. Rev. Lett., 37, 648 (1976).
3. S. Weinberg, Phys. Rev. D5, 1412 (1972).
4. T.D. Lee and C.N. Yang, Phys. Rev. 126, 2239 (1962).
5. The neutrino and Antineutrino Spectra have been calculated by T. Tso at Brookhaven National Laboratory using the Sanford-Wang parametrization of $\pi$ and K production spectra (BNL 11299 JRS/CLW - 1 and JRS/CLW - 2).
6. For a detailed discussion of the implications of our data for models which describe $\nu_\mu p$ elastic scattering, see C.H. Albright, C. Quigg, R.E. Shrock, and J. Smith, Phys. Rev. D14, 1780 (1976); D.P. Sidhu, Phys. Rev. D14, 2235 (1976); E. Fisohbach, J.T. Gruenwald, S.P. Rosen, and H. Spivack, Phys. Rev. Lett. 37, 582 (1976).


## FIGURE CAPTIONS

Fig. 1. Brookhaven neutrino and antineutrino spectra. The $\nu_\mu$ spectrum peaks at $\sim 1.0$ GeV and falls off by one-half at 0.3 GeV and 2.0 GeV; the $\bar{\nu}_\mu$ spectrum peaks $\sim 0.8$ GeV and falls by one-half at 2.2 GeV.

Fig. 2. (a) Side view of Harvard-Pennsylvania-Wisconsin detector showing a typical recoil proton event.

(b) Diagram of a single calorimeter module.

Fig. 3. Comparison of the calculated (for pion and proton hypotheses) energy loss, dE/dZ, with that observed for a 225 MeV particle moving at an angle of $30^\circ$ through the liquid. Pion hypothesis is favored.

Fig. 4. Comparison of calculated energy loss, dE/dZ, with observed for a 299 MeV particle moving at an angle of $25^\circ$. Proton hypothesis is favored.

Fig. 5. Plot of proton kinetic energy versus proton angle for $\nu_\mu p \rightarrow \nu_\mu p$

candidates. A typical error bar shows the uncertainty in the energy (± 10%) and in the angle (± 15°, systematic and stalistical).

Fig. 6. (a) Timing distribution of events during the 3 $\mu$sec beam spill. The 12 peaks are associated with the RF structure of the accelerator which delivers 30 nsec proton bunches separated by 220 nsec.
(b) Fine timing distribution of events. Time from center of RF associated bunch is plotted for $\nu_\mu p$ elastic candidates (cross-hatched) and observed $\nu_\mu p \rightarrow \mu^- p$ quasi-elastic events. The neutrino induced signal lies within ± 30 nsec; flat out of time potential neutron background underlies this signal.

Fig. 7. (a) Transverse event distribution for $\nu_\mu p \rightarrow \nu_\mu p$ candidates.
(b) Longitudinal event distribution for $\nu_\mu p \rightarrow \nu_\mu p$ candidates.

Fig. 8. Detection efficiency corrected $Q^2$- distribution for 30 $\nu_\mu p \rightarrow \nu_\mu p$ events ( 7 background) normalized to CC reaction $\nu_\mu n \rightarrow \mu^- p$.[1]
(b) Preliminary, unnormalized detection efficiency corrected $Q^2$ - distribution for ~ 150 $\nu_\mu p$ elastic candidates.

Fig. 9. (a) Detection efficiency corrected $Q^2$ - distribution for 22 $\bar{\nu}_\mu p \rightarrow \bar{\nu}_\mu p$ events (8 background) normalized to CC reaction $\bar{\nu}_\mu p \rightarrow \mu^+ n$.[2]
(b) Preliminary, unnormalized detection efficiency corrected $Q^2$ - distribution for ~40 $\bar{\nu}_\mu p$ elastic candidates.

Fig. 10. Plot of $R_{\bar{\nu}}$ versus $R_\nu$ for various values of the Weinberg angle. Curves for the Weinberg-Salam model and a pure Vector-like model are shown with our values of $R_\nu$ and $R_{\bar{\nu}}$ which are compatible with the former but not the latter theory.

Acknowledgement: I would like to thank Mr. Mike Burka and Mr. Mark Levine for their valuable assistance with pattern-recognition and programming.

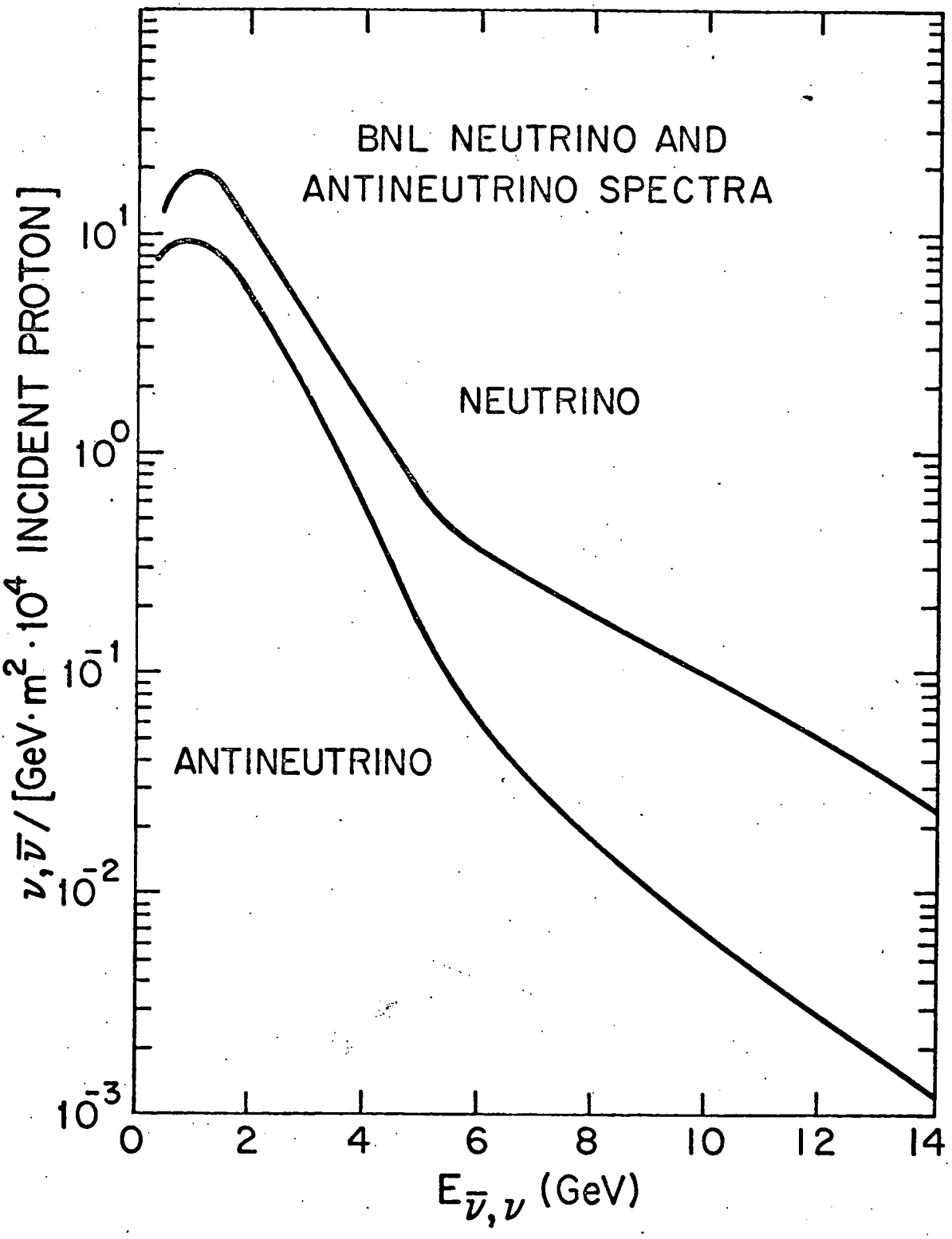
BNL NEUTRINO AND
ANTINEUTRINO SPECTRA
NEUTRINO
ANTINEUTRINO
$\nu, \bar{\nu}$ / [GeV·m$^2$·10$^4$ INCIDENT PROTON]
$10^1$
$10^0$
$10^{-1}$
$10^{-2}$
$10^{-3}$
0
2
4
6
8
10
12
14
$E_{\bar{\nu},\nu}$ (GeV)

Figure 1

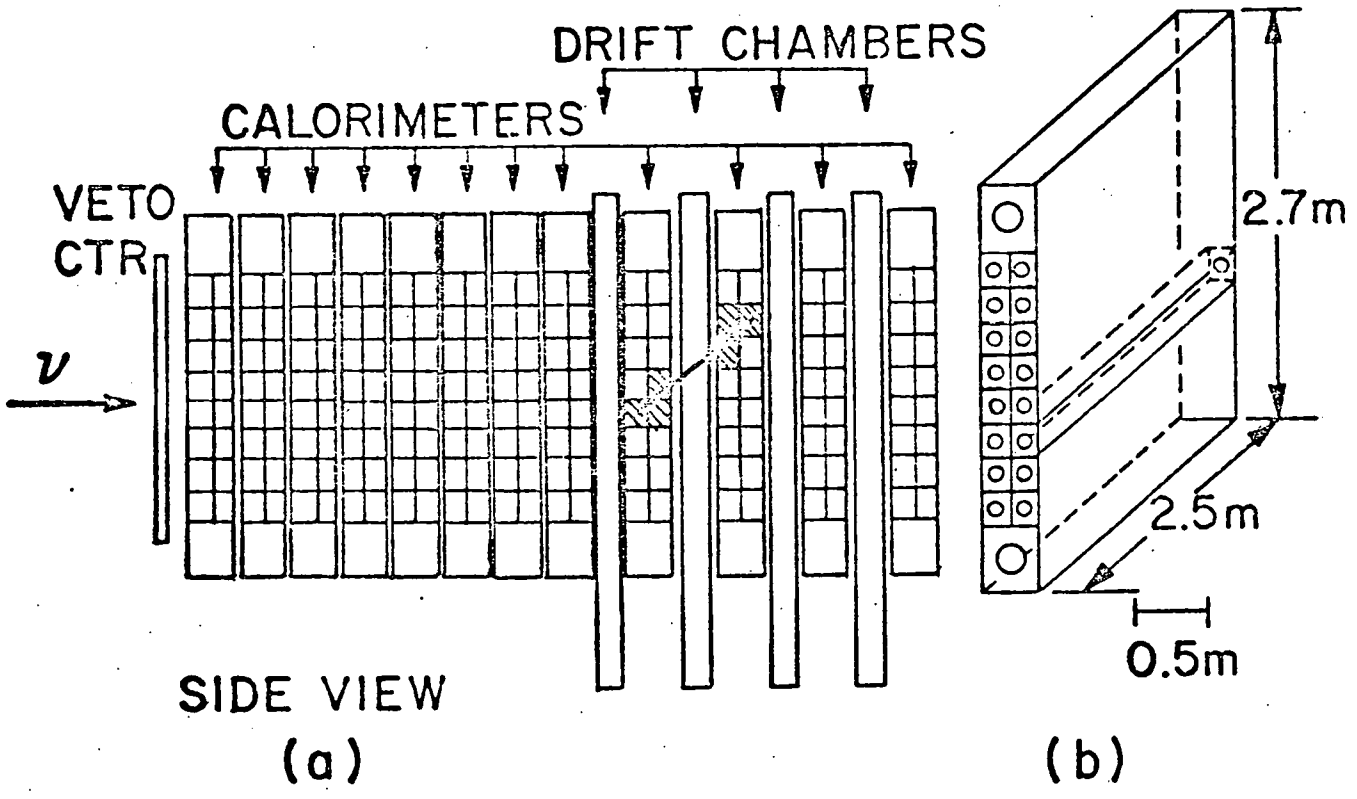
DRIFT CHAMBERS
CALORIMETERS
VETO
CTR
ν
SIDE VIEW
(a)
2.7m
2.5m
0.5m
(b)

Figure 2

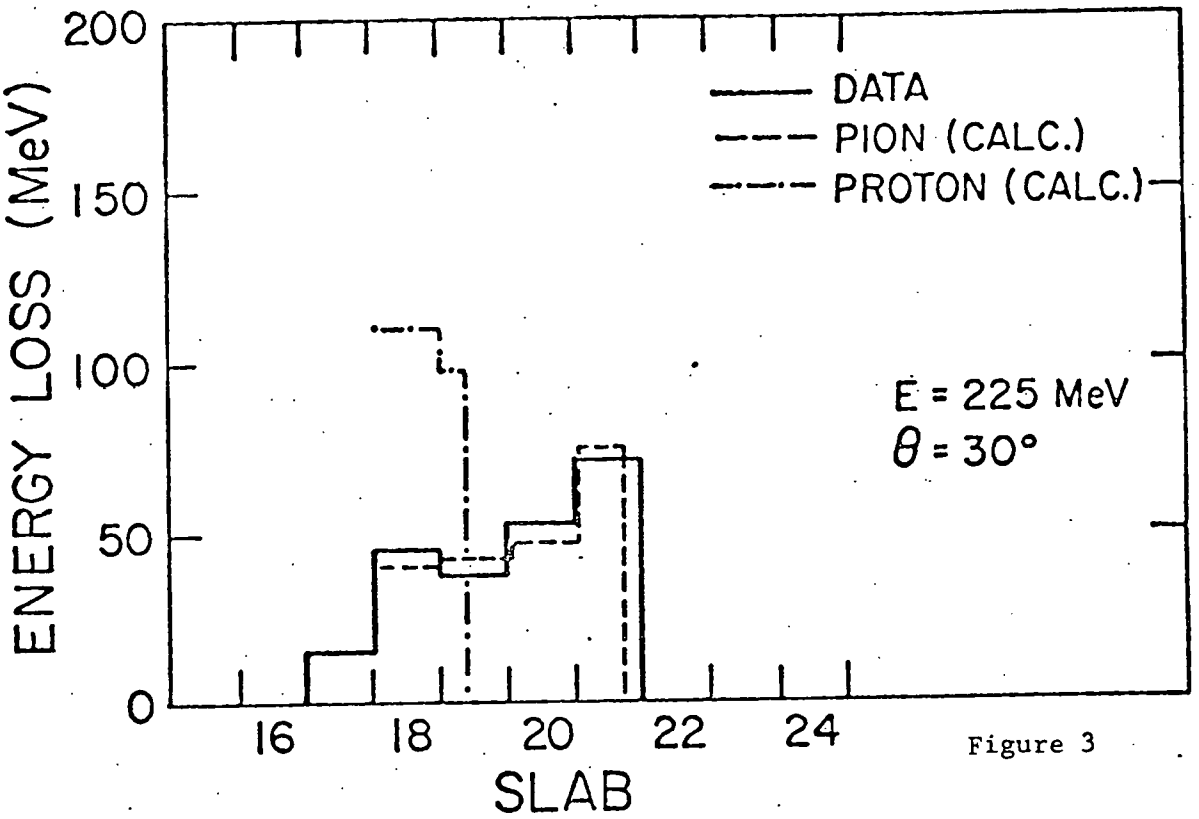


Figure 3

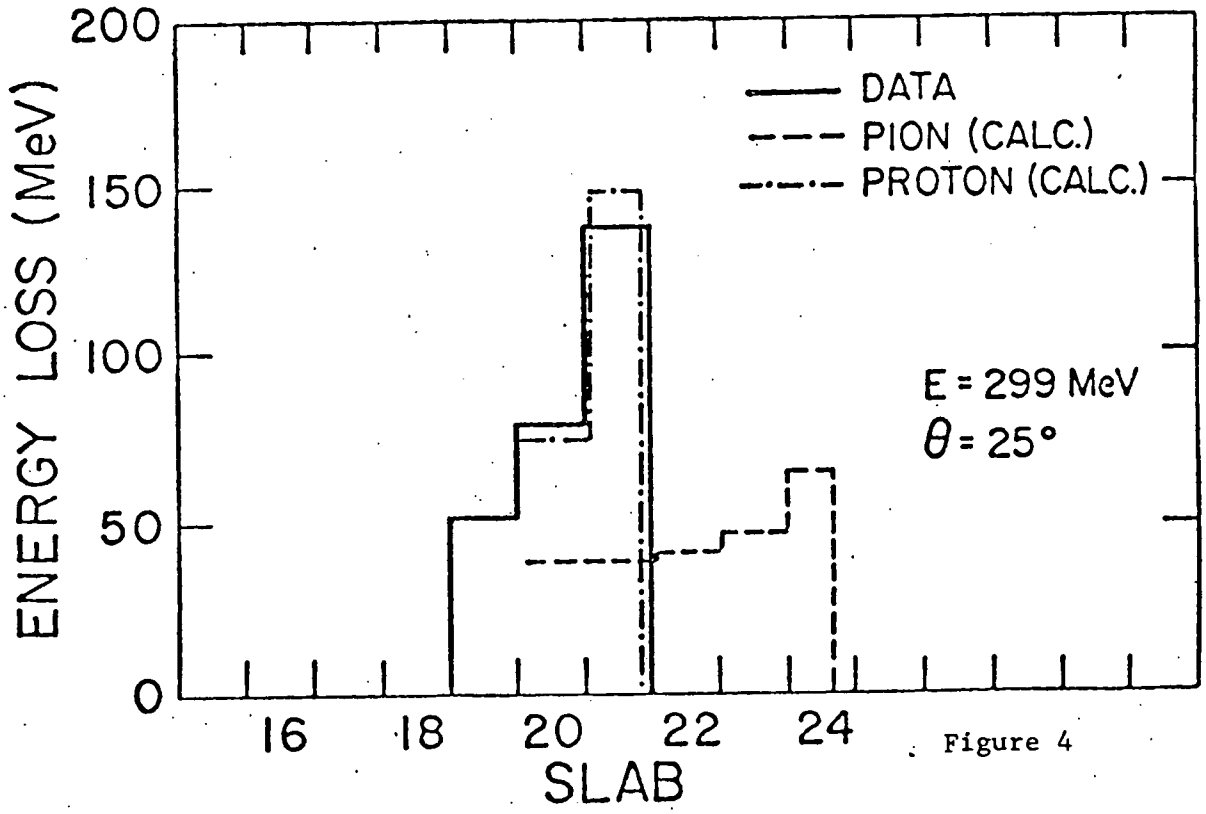


Figure 4

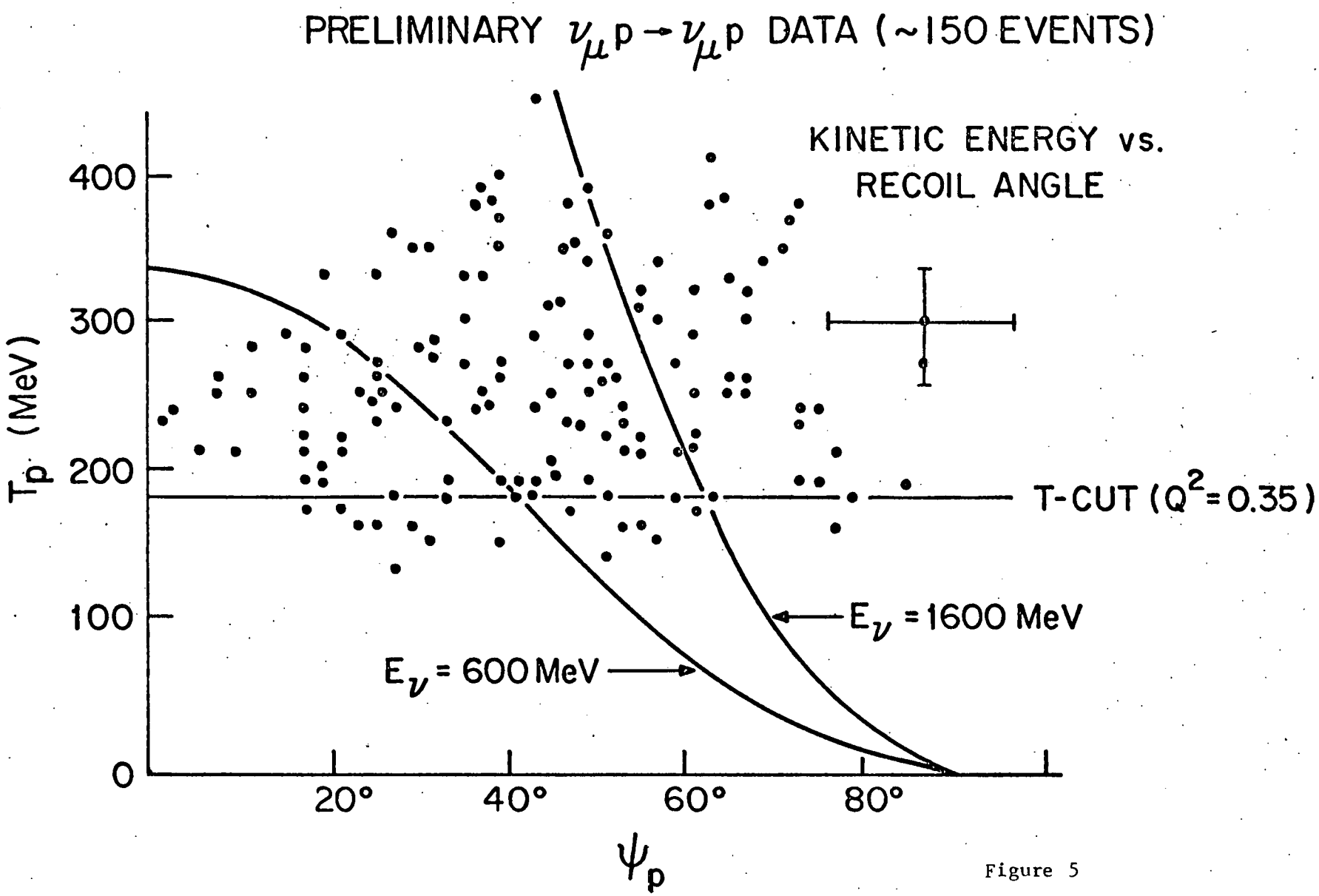
PRELIMINARY $\nu_\mu p \to \nu_\mu p$ DATA (~150 EVENTS)
KINETIC ENERGY vs.
RECOIL ANGLE
400
300
200
100
0
$T_p$ (MeV)
20°
40°
60°
80°
$\psi_p$
T-CUT ($Q^2$=0.35)
$E_\nu$ = 1600 MeV
$E_\nu$ = 600 MeV

Figure 5

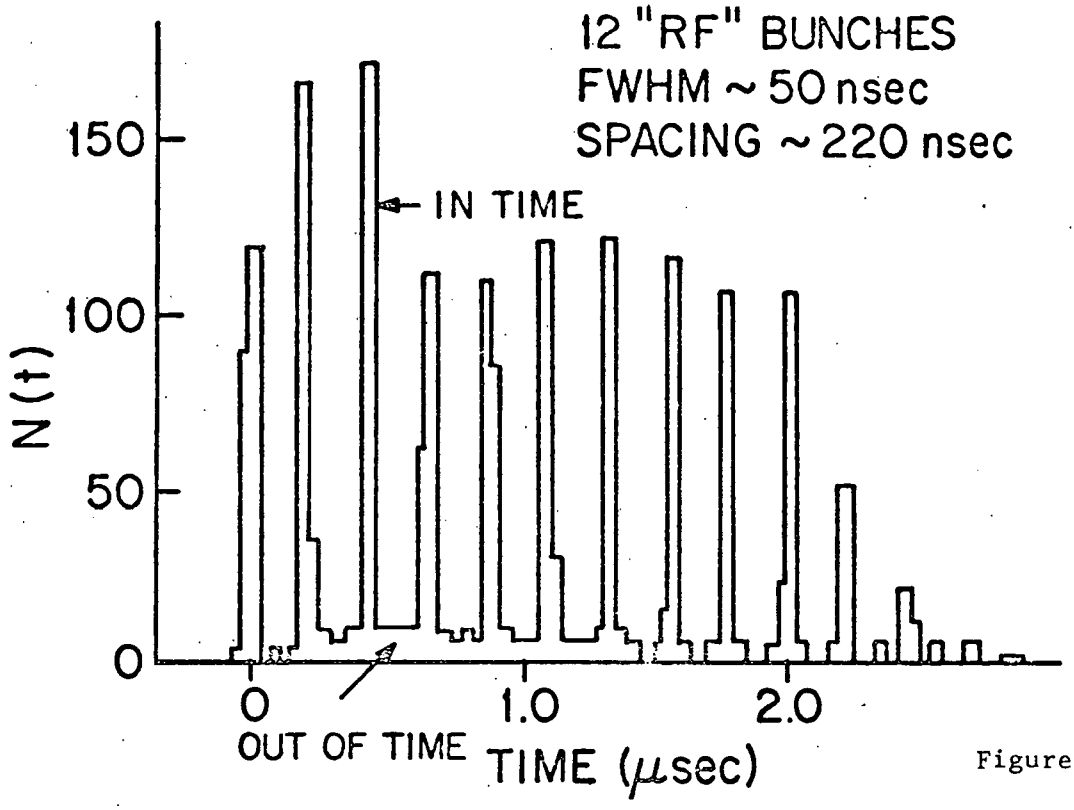


Figure 6a

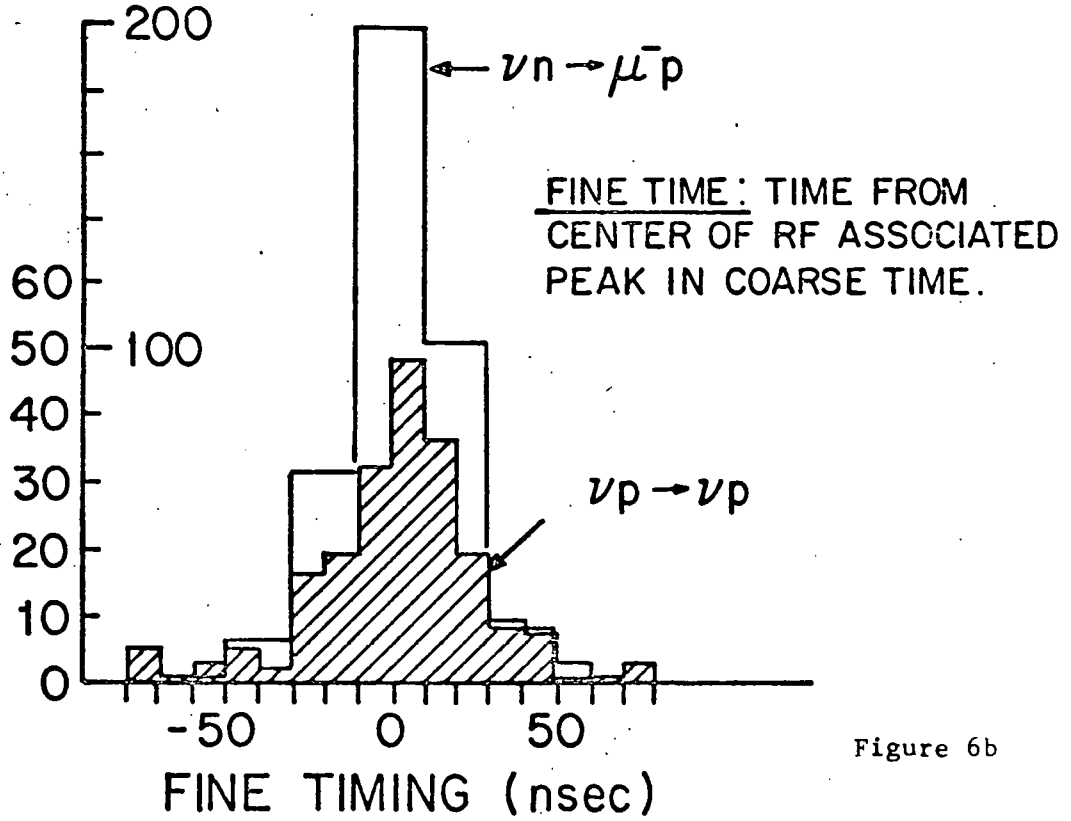


Figure 6b

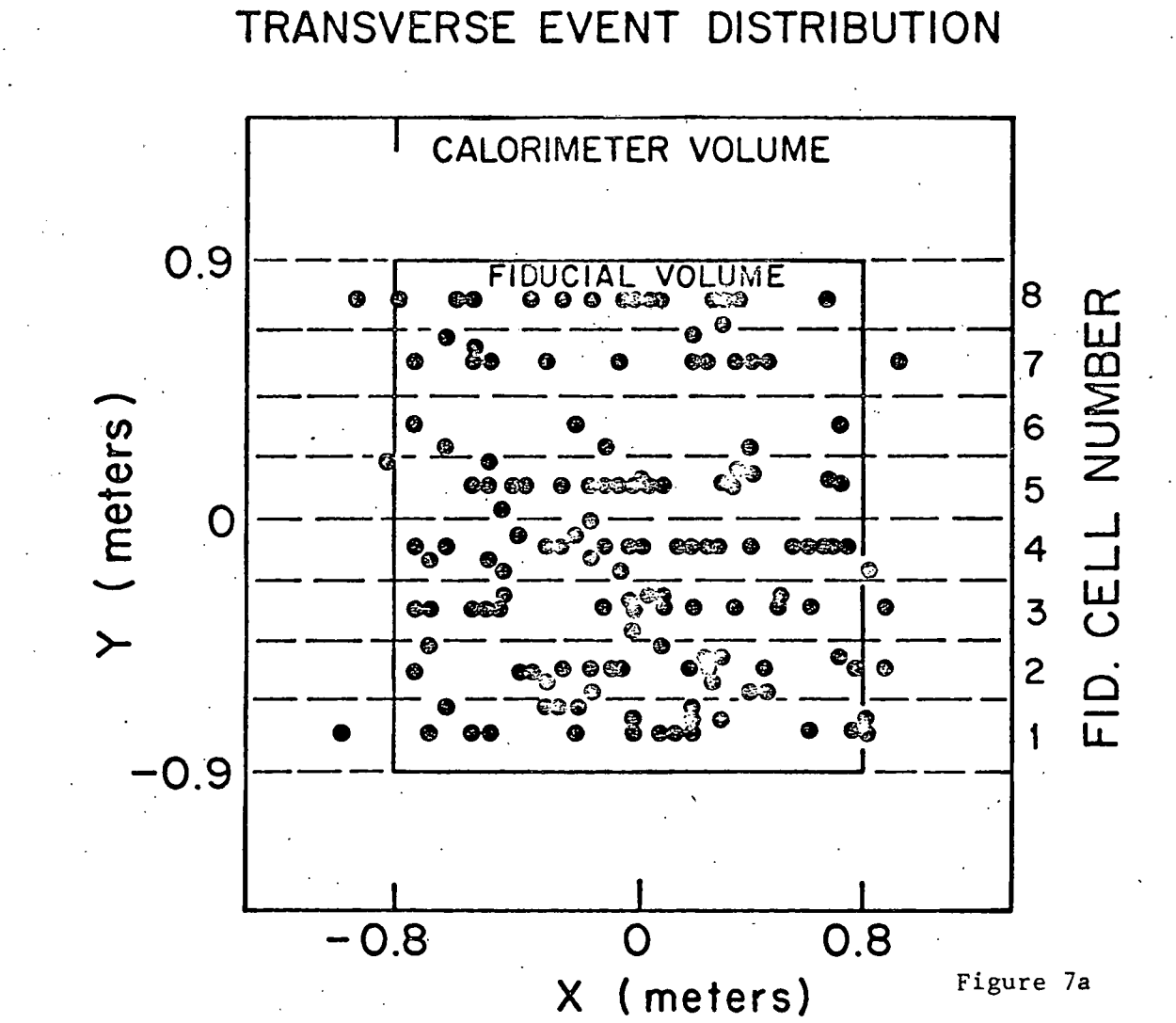


Figure 7a

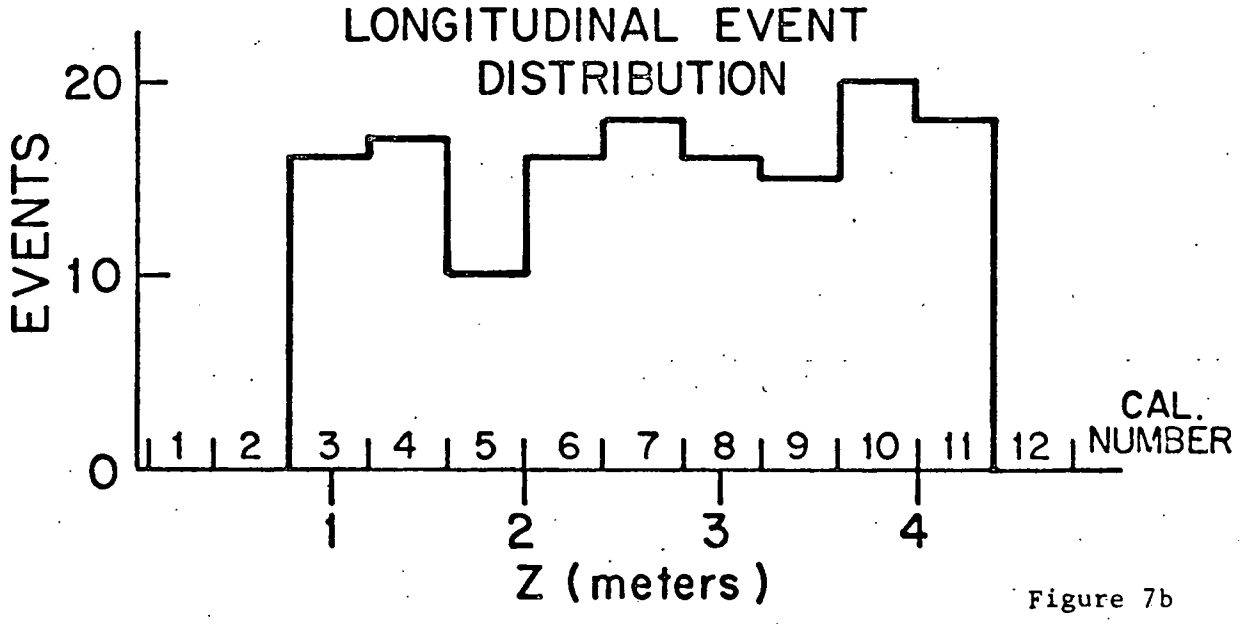


Figure 7b

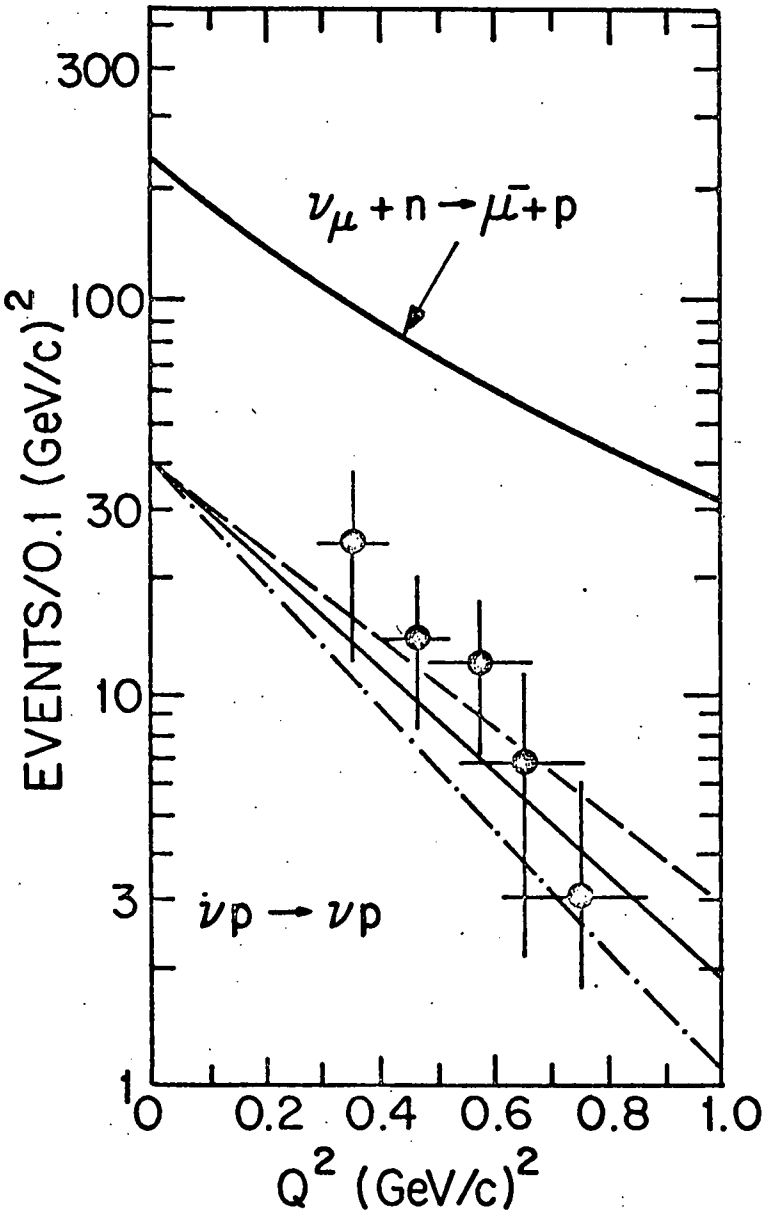


Figure 8a

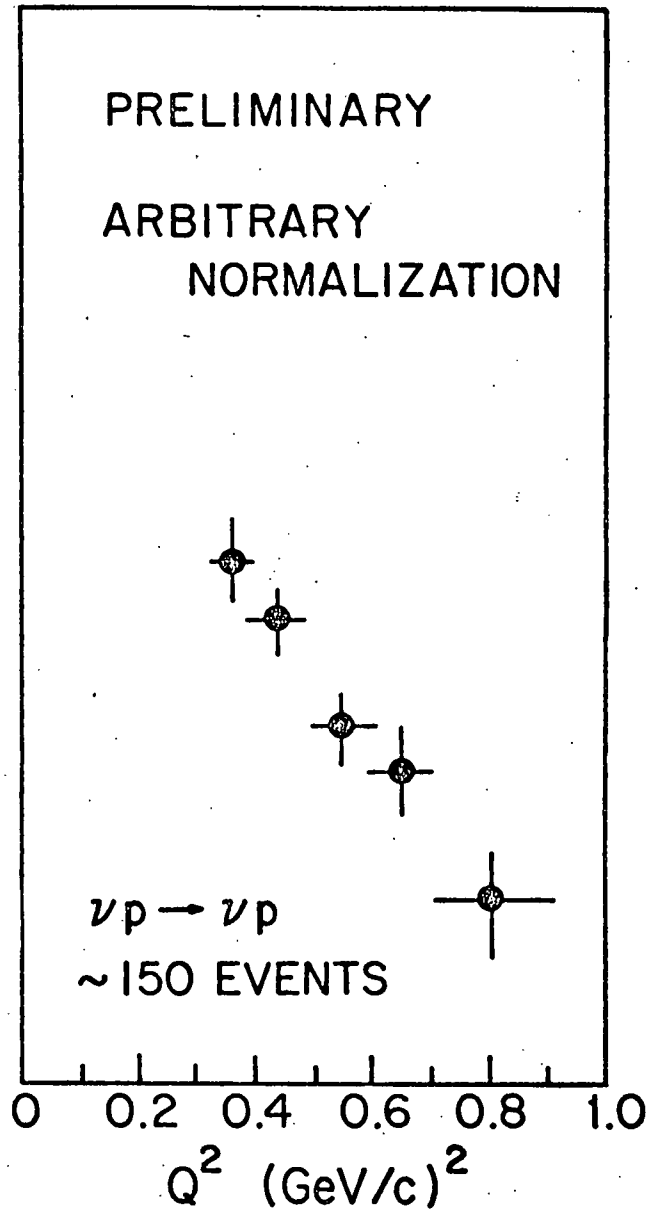


Figure 8b

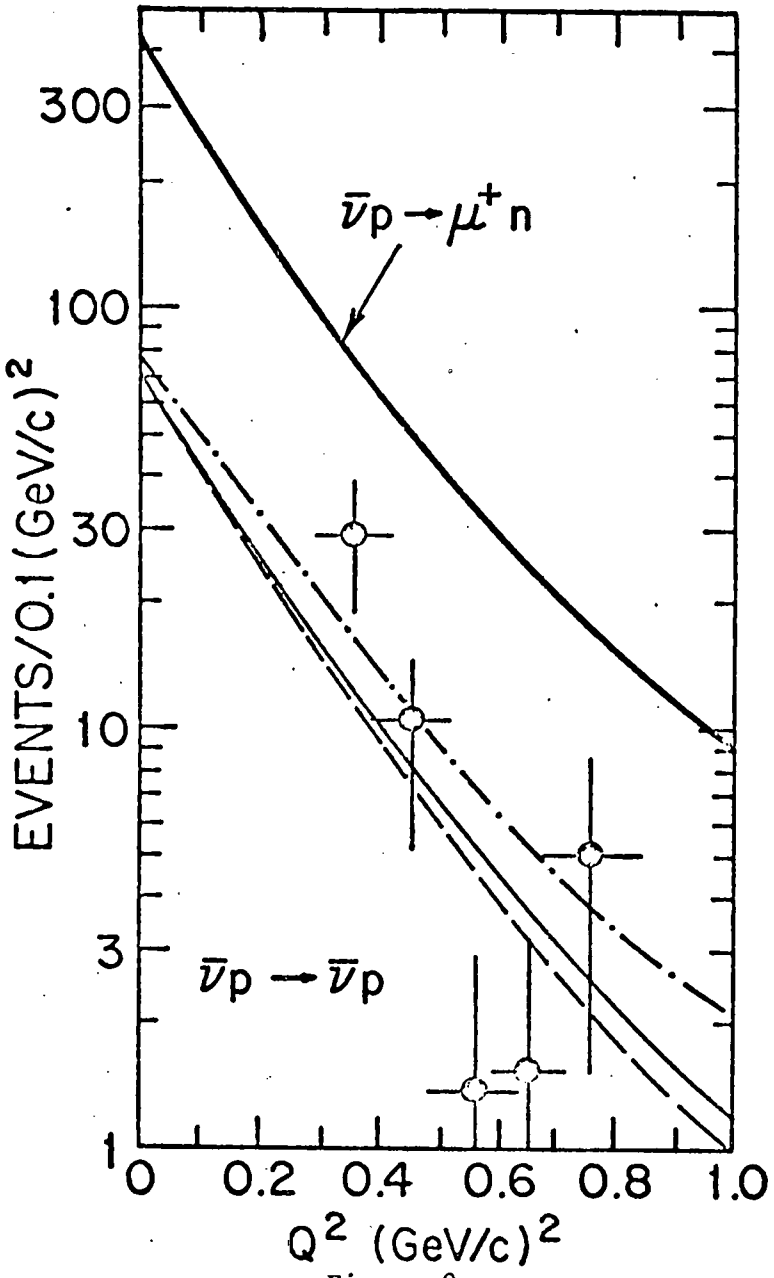


Figure 9a

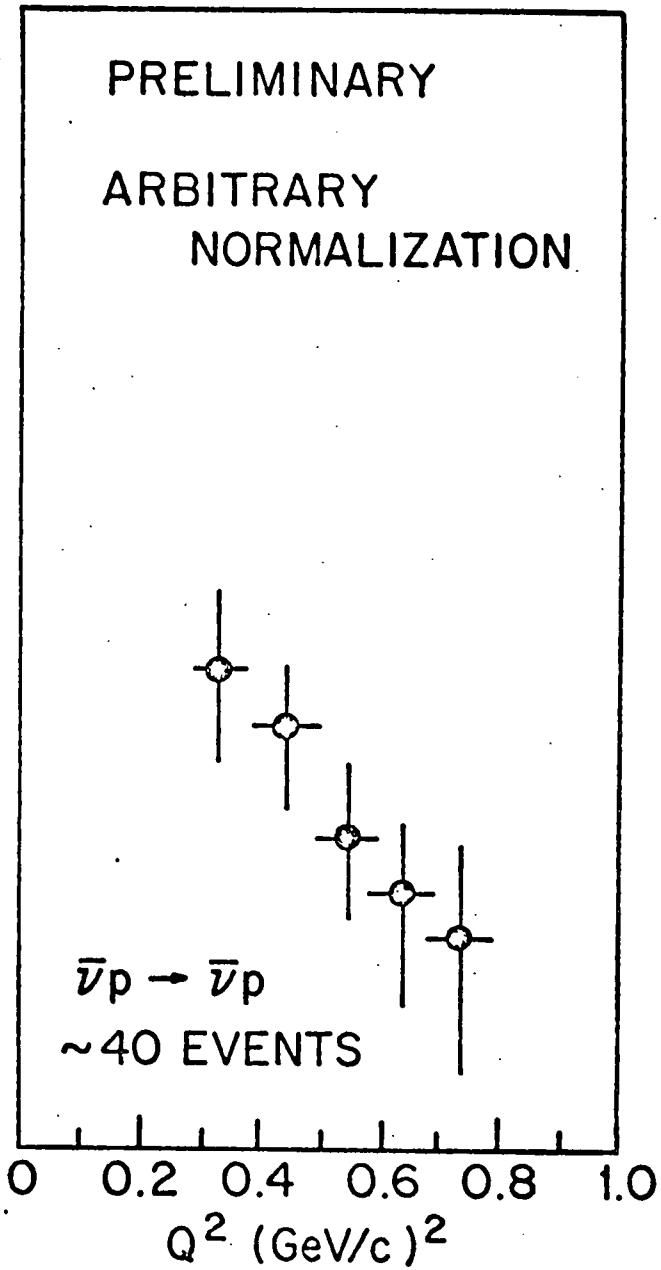


Figure 9b

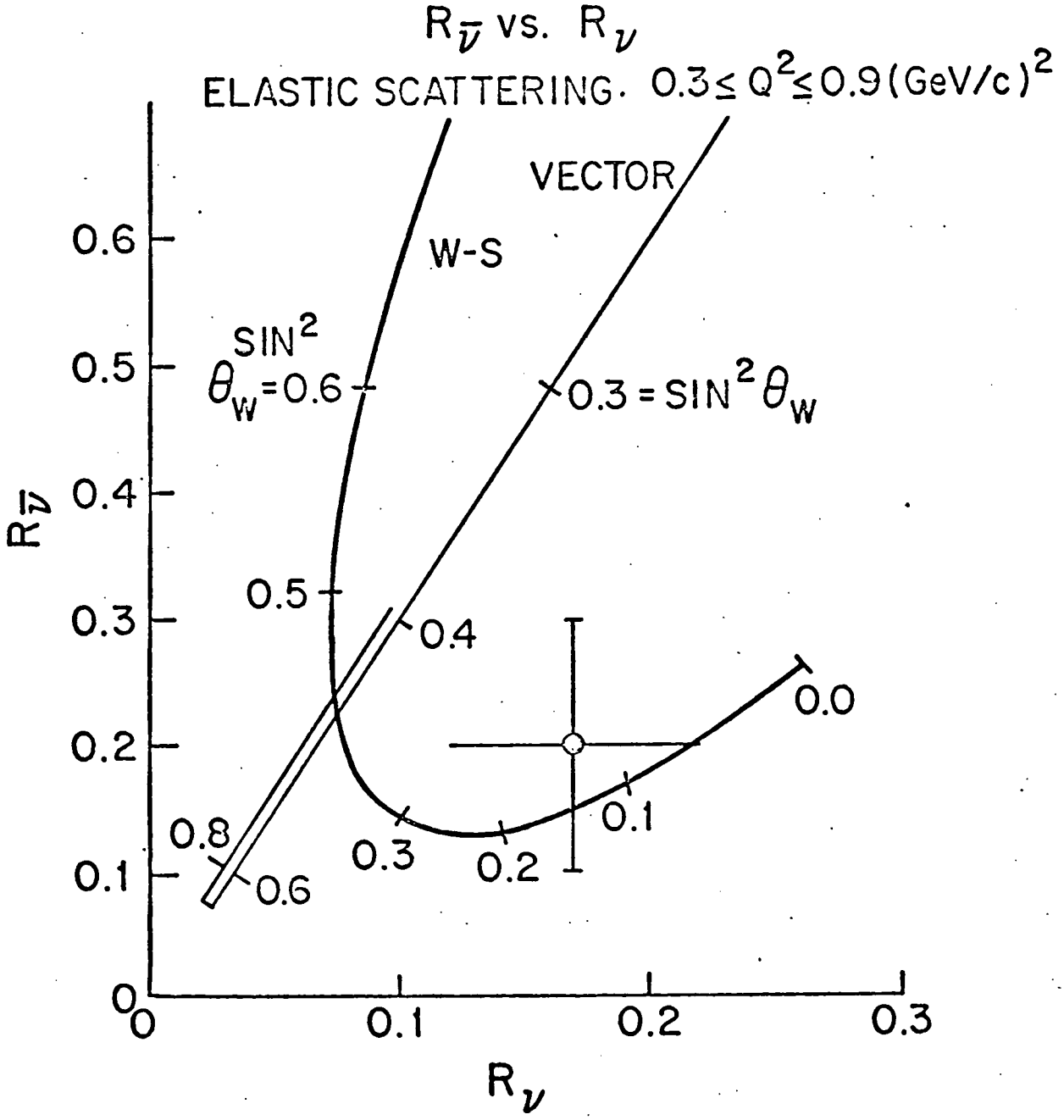
$R_{\bar{\nu}}$ vs. $R_{\nu}$
ELASTIC SCATTERING. $0.3 \leq Q^2 \leq 0.9 (GeV/c)^2$
VECTOR
W-S
$SIN^2 \theta_W = 0.6$
$0.3 = SIN^2 \theta_W$
0.6
0.5
0.4
0.3
0.2
0.1
0
$R_{\bar{\nu}}$
0.5
0.4
0.0
0.8
0.6
0.3
0.2
0.1
0
0.1
0.2
0.3
$R_{\nu}$

Figure 10